Journal of Low Temperature Physics (2022) 207:85–96
https://doi.org/10.1007/s10909-022-02701-3

Vortex Matter in a Two-Band SQUID-Shaped Superconducting film

C. A. Aguirre[1,2] · Julián Faúndez[2] · S. G. Magalhães[2] · J. Barba-Ortega[3,4]

Received: 1 November 2021 / Accepted: 16 February 2022 / Published online: 8 March 2022

Abstract
In the present work, we studied the magnetization, vorticity, Cooper pairs density, and the spatial distribution of the local magnetic field in a three-dimensional superconductor with a SQUID geometry (a square with a central hole connected to the outside vacuum through a very thin slit). Our investigation was carried out in both the Meissner-Ochsenfeld and the Abrikosov state solving the two-band Ginzburg-Landau equations considering a Josephson coupling between the bands. We found a non-monotonic vortex behavior and the respective generation of vortex clusters due to the Josephson coupling used between condensates.

Keywords SQUID · Two bands · Magnetization · Vorticity · Vortex state · Magnetic field perfil

1 Introduction

The application of superconducting technology in different nano- and mesoscopic systems has been of great importance in recent years [1, 2]. Special interest has been placed on the low-temperature superconductors (LTS) which have been used in various applications; among them, the production of magnets with high magnetic fields in the range of $5 - 10\ T$ [3], which are used in particle accelerators and magnetic resonance devices [4]. Furthermore, LTS's are used in the manufacture of high-precision superconducting electronic devices such as microwaves detectors,

✉ C. A. Aguirre
cristian@fisica.ufmt.br

[1] Departamento de Física, Universidade Federal de Mato-Grosso, Cuiabá, Brasil

[2] Condensed Matter Physics Group, Instituto de Fisica, Universidade Federal do Rio Grande do Sul, Porto Alegre, RS 91501-970, Brazil

[3] Departamento de Física, Universidad Nacional de Colombia, Bogotá, Colombia

[4] Foundation of Researchers in Science and Technology of Materials, Bucaramanga, Colombia

superconducting quantum interference devices (SQUID), etc [5, 6]. Due to an increase in the application of different superconducting devices, such devices are expected to show an increase in critical temperatures T_c, to the so-called high critical temperature superconductors (HTCS). These implementations range from the application to the management and treatment of extensive databases, to solutions for mobility in high-speed trains around the world. However, the most widely used magnetometer is the SQUID, since it allows measuring even very slight magnetic fields.

The discovery of superconductivity in MgB_2 in 2001 [7] opened the door to analyze and try to understand unconventional superconductivity. Numerous experiments revealed unconventional results such as a shoulder in the specific heat C at several temperatures, or a positive curvature of the upper critical field near T_c. These results initiated a lot of theoretical investigations of the two-band systems. Today attention has been diverted to iron-based superconductors. Their unconventional behavior is partly different from that of MgB_2, which may be due to quite different Fermi surfaces and gap structures. Theoretical work on the MgB_2 and iron-based materials systems are anticipated to be a powerful tool to understand the multi-band effects. The two-band behavior can be explained from the anisotropy in the sample, from gap-symmetries different from s-wave, and from a second superconducting phase, among other effects. So, we can say that non-conventional behaviors originating from two-band effects are due to the variations of the gap values or the Fermi velocities.

A SQUID can be made from a high critical temperature superconductor, such as a cuprate [8–12] which has a critical temperature $T_c \approx 92K$ [12], alloys $Nb/Al - AlO_x$, $Bi_{1-x}Sb_x2Se_3$ or topological insulator (TI) nano-ribbon (NR) connected with $Pb_{0.5}In_{0.5}$ superconducting electrodes [13–18]. Additionally, an attempt has been made to adapt and apply this multi-band system to other problems with various techniques that have allowed one to study theoretically the vortex state. For example, Rogeri *et al.*, using a genuinely three-dimensional approach to the time-dependent Ginzburg–Landau theory, studied the local magnetic eld profile of a mesoscopic superconductor in the so-called SQUID geometry. They studied the magnetic induction in both the Meissner and the mixed state as a function of temperature [19]. Brandt *et al.*, using the London theory, calculated dynamic electromagnetic properties in thin flat superconducting films of rectangular and circular films without and with slits and holes. The sheet currents and the coupling between the vortices and the defects were expressed by a stream function. They found that due to the long-ranging magnetic stray field, the interaction energy between vortices and the magnetic field depends on the size, the cross-section of the sample, and shape of the film [20–22].

The influence of the boundary conditions on the magnetization curve of the sample in a thin mesoscopic superconductor in the SQUID geometry (circular with a hole at the center connected to the outer rim by a very thin slit) was studied in the reference [23]. They found that the first vortex penetration field and vorticity strongly depend on the boundary condition. H. J. M. ter Brake *et al.*, made an interesting roadmap that describes in a general way the developments of superconducting digital electronics under simulations and circuit design, circuit manufacturing, and new devices and

materials [24]. T. Noh *et al.*, described a SQUID in which the Josephson junctions are formed from strips of normal metal in contact with a superconductor. They measured the flux dependence of the critical current of this system without applying a finite voltage bias across the Superconductor-metal normal-superconductor junction, enabling sensitive flux detection without generating microwave radiation [25]. M. Mori *et al.*, studied the π–SQUID comprising 0– and π– Josephson junctions, they found that the π–SQUID can be a π–Qubit with spontaneous loop currents by which the half-integer Shapiro-Steps are induced, then the 0– and π–Josephson junctions equivalent is a key for the half-integer Shapiro-Steps and realizing the π–Qubit [26]. Thus, it is difficult to reiterate the extensive importance of this measurement instrument. However, we propose an extension in the manufacture of the same device, but in a two-band extension considering a Josephson type coupling between them. This extension generates a non-monotonic behavior between the vortices and the creation of vortex clusters.

This article is organized as follows: the theoretical formalism is presented in Sect. 2. In Sect. 3, we present the main results for the studied system. We show the vortex states, vorticity, magnetization, and profile of the magnetic induction as functions of external magnetic field **H** for a mono and two-band three-dimensional SQUID. Finally, in Sect. 4 we detail the main results.

2 Theoretical Formalism

In this work, we studied the vortex matter in a mesoscopic superconductor in the so-called SQUID geometry, through the functional of a two-band superconductor system. We will consider the interaction between the two bands (or condensates ψ_1, ψ_2) in a Josephson-type coupling. Thus, the Gibbs energy for the superconducting order parameter complex pseudo-function $\psi_i = |\psi_i| e^{i\theta_i}$ (θ_i its phase) [27–30], and magnetic potential **A**, where $\mathbf{B} = \nabla \times \mathbf{A}$, is:

$$\mathcal{G} = \int dV \left(\sum_i^2 \mathcal{F}(\psi_i, \mathbf{A}) + \frac{1}{2\mu_0} |\nabla \times \mathbf{A}|^2 + \Theta(\psi_i) \right) \tag{1}$$

where:

$$\mathcal{F}(\psi_i, \mathbf{A}) = \alpha_i |\psi_i|^2 + \frac{\beta_i}{2} |\psi_i|^4 + \frac{\zeta_i}{2m_i} |(i\hbar\nabla + 2e\mathbf{A})\psi_i|^2 \tag{2}$$

and

$$\Theta(\psi_1, \psi_2) = \gamma(\psi_1^* \psi_2 + \psi_2^* \psi_1) \tag{3}$$

$\alpha_i = \alpha_{i0}(1 - T/T_{ci})$ and β_i are two phenomenological parameters, $i = 1, 2$ in the equations 1 and 2. We used the Josephson coupling showed in the equation 3. In the London gauge $\nabla \cdot \mathbf{A} = 0$, we express the temperature T in units of the critical temperature T_{c1}, length in units of the coherence length $\xi_{10} = \hbar/\sqrt{-2m_1\alpha_{10}}$, the order parameters in units of $\psi_{i0} = \sqrt{-\alpha_{i0}/\beta_i}$, time in units of the Ginzburg-Landau characteristic time $t_{GL} = \pi\hbar/8k_B T_{c1}$, and the vector potential **A** is scaled by $H_{c2}\xi_{10}$,

where H_{c2} is the bulk upper critical field. The general form of time dependent Ginzburg-Landau equations for a two-band system in dimensionless units [29, 30] is given by:

$$\frac{\partial \psi_1}{\partial t} = (1 - T - |\psi_1|^2)\psi_1 - |\mathbf{D}|^2\psi_1 + \hat{\gamma_1} \tag{4}$$

$$\frac{\partial \psi_2}{\partial t} = \left(1 - \frac{T}{T_{r2}} - |\psi_2|^2\right)\psi_2 - \frac{m_{r2}}{\alpha_{r2}}|\mathbf{D}|^2\psi_2 + \hat{\gamma_2} \tag{5}$$

with:

$$\hat{\gamma_1} = \frac{\gamma|\psi_2|\psi_1}{|\psi_1|}\left[\cos(\theta_2 - \theta_1) + i\sin(\theta_2 - \theta_1)\right] \tag{6}$$

and

$$\hat{\gamma_2} = \frac{\gamma|\psi_1|\psi_2}{|\psi_2|}\left[\cos(\theta_2 - \theta_1) - i\sin(\theta_2 - \theta_1)\right] \tag{7}$$

For more details for the calculus of the relation 6 and the relation 7 (see Ref. [27]). The equations (4) and (5) are solved in Ω_{sc}, while the equation for the vector potential $\mathbf{A}$:

$$\frac{\partial \mathbf{A}}{\partial t} = \begin{cases} \mathbf{J}_s - \kappa^2\nabla\times\nabla\times\mathbf{A} & \text{in } \Omega_{sc} \\ -\kappa^2\nabla\times\nabla\times\mathbf{A} & \text{in } \Omega\backslash\Omega_{sc} \end{cases} \tag{8}$$

are solved in $\partial\Omega_{sc}$, where:

$$\mathbf{J}_s = \zeta_1\Re\left[\psi_1\mathbf{D}\psi_1^*\right] + \zeta_2\Re\left[\frac{\beta_{r2}}{\alpha_{r2}}\psi_2\mathbf{D}\psi_2^*\right] \tag{9}$$

For this case, $\zeta_1 = \zeta_2$, also $\mathbf{D} = i\nabla - \mathbf{A}$. The domain Ω_{sc} is filled by the superconducting parallelepiped of high c and square lateral sizes a and b. The superconducting vacuum interface is denoted by $\partial\Omega_{sc}$. Due to the demagnetization effects, we consider a larger domain Ω of dimensions $A \times B \times C$, such that $\Omega_{sc} \subset \Omega$. The vacuum-vacuum interface is indicated by $\partial\Omega$. The domain Ω is taken sufficiently large such that the local magnetic field equals the applied field $\mathbf{H}$ at the surface $\partial\Omega$ or at $x = \pm A/2$, $y = \pm B/2$, and $z = \pm C/2$ planes. We have studied a mesoscopic superconducting parallelepiped in the domain Ω_{sc} of height $c = 1\xi$ and lateral dimension $a = b = 12\xi$; the central hole has dimensions $2.4\xi \times 2.4\xi$. In order to solve the 3D Ginzburg-Landau equations, the size of the simulation box Ω was taken $C = 11\xi$, $A = B = 19\xi$. The grid space used was $\Delta_x = \Delta_y = \Delta_z = 0.25\xi$ (see reference [31] for more details).

$\hat{\gamma}_1, \hat{\gamma}_2$ represents the Josephson coupling between the i and j band. The boundary conditions $\mathbf{n}\cdot(i\boldsymbol{\nabla} + \mathbf{A})\psi_i = 0$, $i = 1, 2$ with $\mathbf{n}$ a surface normal outer vector. Also, we defined $m_{r2} = m_2/m_1 = 0.5$, $\beta_{r2} = \beta_2/\beta_1 = 0.7$, $\gamma = -0.01$, $\zeta_1 = \zeta_2 = 0.01$, $\kappa = 5.0$, simulating a MgB_2 sample [32]. We choose the zero-scalar potential

gauge at all times and use the link variables method to solve the Ginzburg-Landau equations [32–37] (and references therein).

3 Numeric Results

In Fig. 1, we present the layout of the studied sample. It is a SQUID in a perpendicular external applied magnetic field $\mathbf{H}$ with dimensions $c = 1\xi$, $a = b = 12\xi$; the central hole has dimensions $2.4\xi \times 2.4\xi$. We show the magnetization $-4\pi\mathbf{M}$, vorticity N, superconducting electronic density for the band 1 $|\psi_1|^2$, and for the band 2 $|\psi_2|^2$, respectively and the profile of the magnetic induction $\mathbf{B}$ in (x, $b/2$, $c/2$) plane as a function of the external applied magnetic field $\mathbf{H}$ when is increasing and decreasing. This loop in the magnetic field, aims to describe a hysteresis cycle and computationally the magnetic field will vary between $0 \leq \mathbf{H} \leq \mathbf{H}_2$, ($\mathbf{H}_2$ is the upper magnetic field, where we found that $\mathbf{H}_2 = 2.0$ for the single-band sample and $\mathbf{H}_2 = 1.8$ for the two-band sample). Finally for magnetization, we will use $\mathbf{M} = \mathbf{H} - \mathbf{B}/4\pi$, for $\mathbf{H}$ and $\mathbf{B}$ the average value in the sample is taken. For the vorticity or vortex number, we use $N = Im(\psi_i \nabla \psi_i^*)/(\psi_i^* \psi_i)$, with $i = 1, 2$, indicating the band index.

3.1 Single-Band SQUID

In Fig. 2, we present the magnetization $-4\pi\mathbf{M}$, for the single-band SQUID system in a loop of the magnetic field. We observe that for the upward branch of the magnetic field, the behavior of the magnetization is conventional. On the other hand in the downward branch of the loop, we observe that the sample does return to the starting point. Additional in $0 < \mathbf{H} < \mathbf{H}_1$, ($\mathbf{H}_1 \approx 0.7$ is the lower critical field), the sample is in Meissner-Ochsenfeld state in the upward branch of $\mathbf{H}$ and $0 < \mathbf{H} < 0.12$ in the downward branch of $\mathbf{H}$. This behavior has already been studied, and in general terms, it is that of a conventional superconducting sample.

In Fig. 3, we present the vorticity N as a function of the applied magnetic field $\mathbf{H}$. We observe the quantized entrance of the magnetic flux in the sample, when having pinning centers into the sample, we observe that in the upward branch, the sample presents a different number of vortices, accounting for the anchoring of vortices by the barrier of energy between the sample and the pinning. Additionally, note that

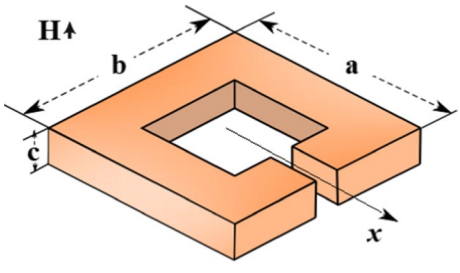

Fig. 1 Layout of the studied sample in a perpendicular external applied magnetic field $\mathbf{H}$. $c = 1\xi$, $a = b = 12\xi$; the central hole has dimensions $2.4\xi \times 2.4\xi$ (Color figure online)

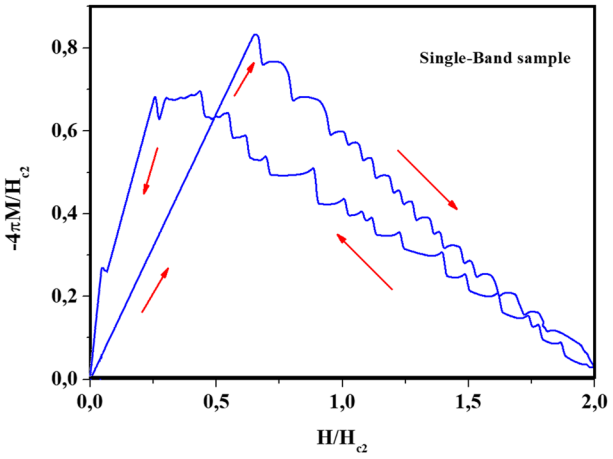

Fig. 2 Magnetization $-4\pi\mathbf{M}$ as a function of the external applied magnetic field $\mathbf{H}$ in the upward branch and downward branch for a single-band Squid (Color figure online)

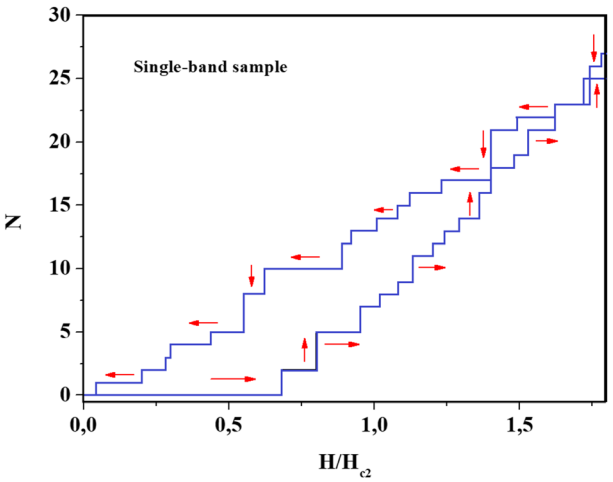

Fig. 3 Vorticity N (or vortex number) as a function of $\mathbf{H}$ in the upward branch and downward branch for a single-band Squid (Color figure online)

the jump in magnetization in Fig. 2, coincides with the in-flux of fluxoids shown in Fig. 3.

Now, in Fig. 4, we show the vortex state ($|\psi|^2$) (or density of Cooper pairs), for the single-band sample as a function of $\mathbf{H}$ in the upward branch (upper panels) and downward branch (lower panels). Thus, by increasing $\mathbf{H}$ we observe the entry of the vortices in the superconducting sample; now, due to the entry of these vortices, there is a competition between the surface energy barrier at the external boundary and the internal pinning. This competition causes the vortices to move in the sample until reaching different positions where the energy is minimized and stabilized in the

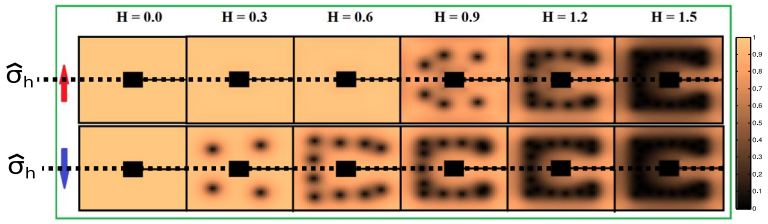

Fig. 4 Square modulus of the order parameter $|\psi|^2$ (density of Cooper pairs/vortex state) as a function of the external applied magnetic field **H** in the upward branch (upper panels) and downward branch (lower panels), for the indicated values of **H** for a single-band Squid sample (Color figure online)

sample (observe a horizontal reflection $\hat{\sigma}_h$ (see figure) when the field increases and decreases for the same **H**). This process is repeated with a greater number of vortices as the external magnetic field **H** increases, we observe that as the field increases, the loss of the superconducting state is evident (conventional behavior).

3.2 Two-Band SQUID

Now, we concentrate on the study of a superconductor SQUID composed of two-bands ψ_1, ψ_2 (or two condensates). To do this, we will start at Fig. 5, where we present the magnetization $-4\pi\mathbf{M}$ curve. Initially, we note that for $0 < H < H_1$, ($H_1 \approx 0.5$ is the lower critical field), it is in the Meissner-Ochsenfeld state and that for $0.5 < \mathbf{H} < 0.8$ there is a non-conventional behavior in the system, having drops in magnetization and a successive increase; initially, we observe that the lower critical fields are different for the single-band and two-band systems; $\mathbf{H}_{1-Single-band} > \mathbf{H}_{1-Two-band}$ and $\mathbf{H}_{2-Single-band} > \mathbf{H}_{2-Two-band}$. After this, the system

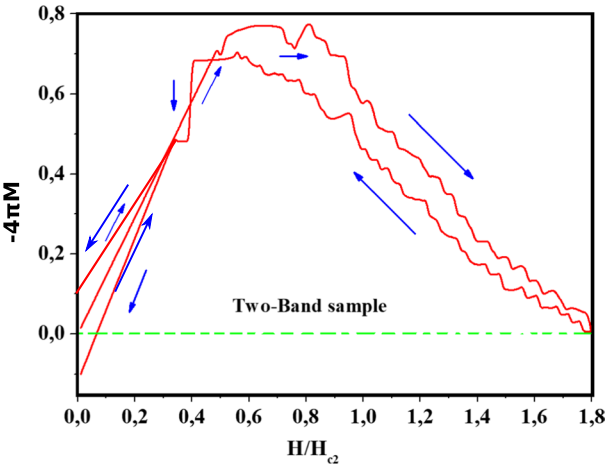

Fig. 5 Magnetization $-4\pi\mathbf{M}$ as function of **H** in the upward branch and downward branch for a two-band Squid system (Color figure online)

behaves similarly to a single-band Squid, in the sense that there are jumps in magnetization, which are indicators of the entry of fluxoids into the sample. In the downward branch of **H** (lower panels), we have a non-conventional behavior, even with very strong variations in the magnetization drops. However, for $-4\pi\mathbf{M}$, we observe the effect of non-homogeneity in the sample, observing the anchoring of vortices in the superconducting sample, an effect due to the competition between the energy barriers in the present system.

Now, in Fig. 6, we present the vorticity N as a function of **H** for bands 1 and 2. Initially, we observe that the vorticity N is different for each of the condensates, with which we expect different vortex states. Now, as the sample is an overlay of the superconducting condensates, the vortex centers are not coincident, giving possible fractional states in the total vortex state (a result of the two-band Josephson coupling type), which allows tunneling of vortices and anti-vortices between superconducting bands. Of greater importance is Fig. 6, where we observe a collective behavior of the two superconducting bands; this means that when the two-band system passes to a normal state at $\mathbf{H}_2 = 2.0$, the phases and the superconducting condensates stabilize and generate behavior in phase, establishing a stable and organized loss of the vortices; as you vary in the upward branch for **H**, this is a novel behavior in a two-band Squid system, where a decrease in vorticity would be expected with different values for each of the condensates.

Now, in Fig. 7, we present the square modulus of the order parameter $|\psi_1|^2, |\psi_2|^2$ or Cooper pairs density for each band. We can see from Fig. 7 that at $\mathbf{H} = 0$, the sample remains in the Meissner-Ochsenfeld state, when the magnetic field increases, the vortices enter through the border of the regions closest to the slit, then they move entering the sample until they reach the normal state at $\mathbf{H}_{c2}$. Then, when the magnetic field decreases, the vortices are expelled from the sample until $\mathbf{H} = 0$ where we found $N = 0$, so, there are not any pinning effects due to the presence of the hole.

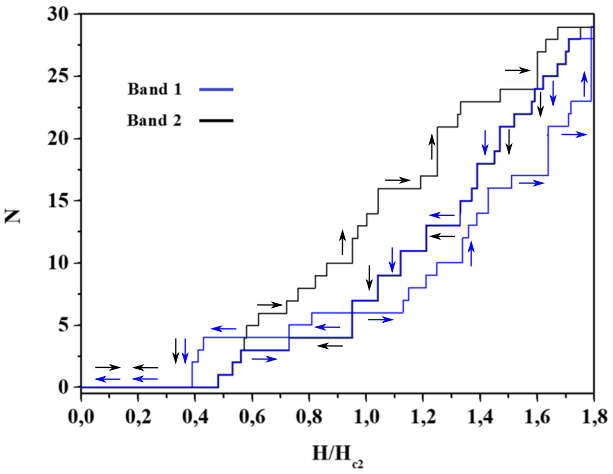

Fig. 6 Vorticity N as a function of **H** in the upward branch and downward branch for a two-band Squid superconductor system (Color figure online)

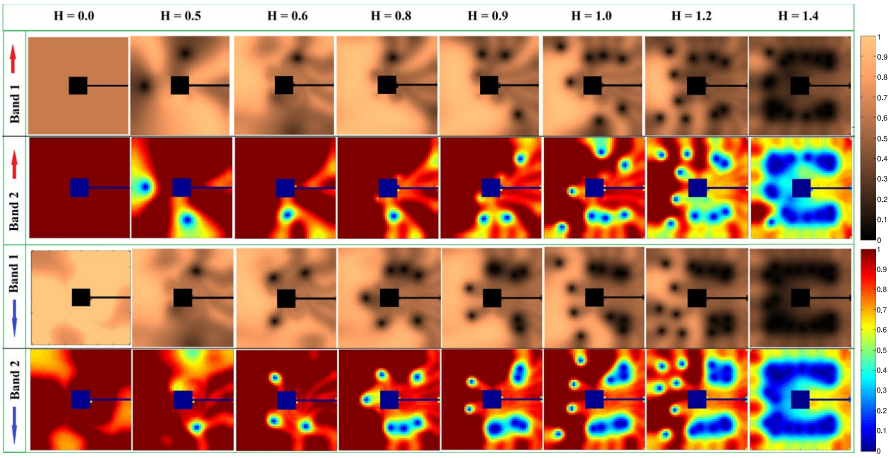

Fig. 7 Square modulus of the order parameter $|\psi_1|^2, |\psi_2|^2$ for the band 1 and the band 2, respectively as a function of **H** in the upward branch (arrow up) and downward branch (arrow down) for the indicated values of **H** (Color figure online)

For some values of the **H** field, there is some observation of specular reflection, we think it is due to the type of coupling, which presents a break in the inversion symmetry [38]. In addition to producing hysteresis in the relaxation of the electronic states present in the superconductor SQUID system.

Now, in Fig. 8, we have plotted the local magnetic field or magnetic induction **B** along the x axis, which passes through the slit and the hole of the SQUID as is shown in Fig. 8, for the indicate values of **H** in the upward branch and downward branch for a two-band case. As can be seen from this graph, the profile of the magnetic field $B_z(x, b/2, c/2)/H$ is very dependent on **H** in both upward branch and downward branch. We found that at the point in which the profile is calculated (x, b/2, c/2), the magnetic induction profile is identical for both bands, that is, the condensates act in phase under the application of an external magnetic field **H**, even though the magnetic field in each condensate presents different values and different vortex states (See Fig. 7).

4 Conclusions

In the present work, we have studied the magnetic properties and vortex state in a superconducting three-dimensional SQUID (single- and two-band) based on a Josephson-type coupling. This study was carried out by solving the Ginzburg-Landau time-dependent equations. We study magnetization, vorticity, vortex state, and profile of the magnetic induction, observing non-conventional behavior of the vortex state in the two-band system. Additionally, we present the typical behavior of the vortex matter for a single-band sample but a non-conventional vortex state for a two-band case, which establishes the existence of non-monotonic interaction between the vortices (short-range repulsion and long-range attraction). Finally, we did not find

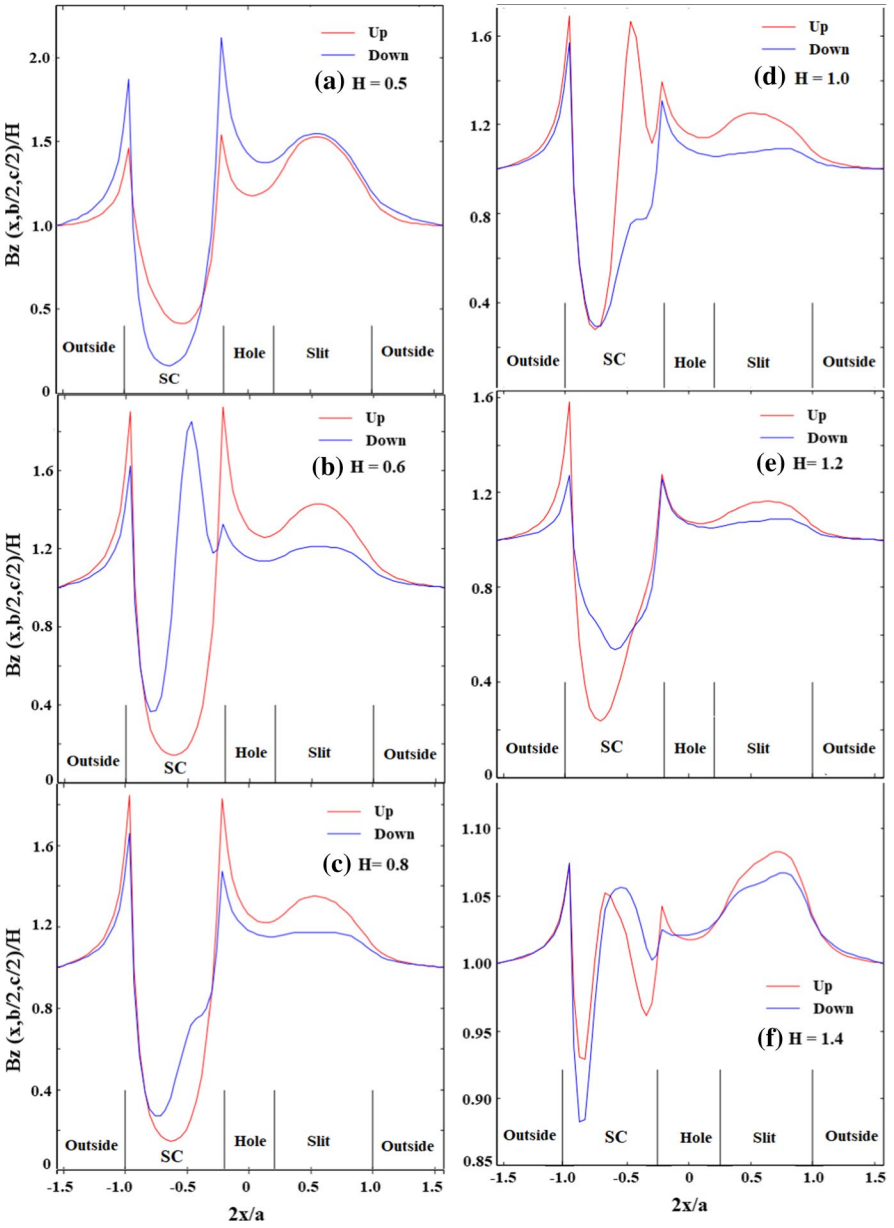

Fig. 8 Intensity of the z component of the magnetic induction **B**, normalized to **H**, along the axis x for indicates values of **H** in the upward branch (up) and downward branch (down) for a two-band Squid. (SC means Superconductor) (Color figure online)

any difference in the magnetic profile of the magnetic induction between the bands. Our results in the mono-band case are in qualitative nature agreement with previous works.

Acknowledgements C. A. Aguirre, would like to thank the Brazilian agency CAPES, for financial support, Grant number: 0.89.229.701-89. J. Faúndez and S. G. Magalhães thank FAPERGS, CAPES and CNPq for partially financing this work under the Grant PRONEX 16/0490-0.

References

1. B.J. Baelus, K. Kadowaki, F.M. Peeters, Phys. Rev. B **71**, 024514 (2005)
2. G.J. Kimmel, A. Glatz, V.M. Vinokur, I.A. Sadovskyy, Sci. Reports **9**, 1 (2019)
3. V.V. Moshchalkov, L. Gielen, C. Strunk, R. Jonckheere, X. Qiu, C. Van Haesendonck, Y. Bruynseraede, Nature **373**, 319 (1995)
4. P.G. de Gennes, *Superconductivity in Metals and Alloys* (Addison-Wesley, Reading, MA, 1989)
5. E. Fillis-Tsirakis, Dissertation at the University of Stuttgart, Max-Planck-Institute for Solid State Research, (2017)
6. J. Clarke, Squid Fundamentals. In: Weinstock H. (eds) SQUID Sensors: Fundamentals, Fabrication and Applications. NATO ASI Series (Series E: Applied Sciences), **329**, Springer, Dordrecht (1996)
7. J. Nagamatsu, N. Nakagawa, T. Muranaka, Y. Zenitani, J. Akimitsu, Nature **410**, 63 (2001)
8. J.R. Kirtley, J.P. Wikswo Jr., Annu. Rev. Mater. Sci. **29**, 117 (1999)
9. R. Jaklevic, J. Lambe, A. Silver, J. Mercereau, Phys. Rev. Lett. **12**, 159 (1964)
10. J.E. Zimmerman, A. Silver, Phys. Rev. **141**, 367 (1966)
11. R. Jaklevic, J. Lambe, J. Mercereau, A. Silver, Phys. Rev. **140**, A1628 (1965)
12. A.P. Malozemoff, J. Mannhart, D. Scalapino, Phys. Today **58**, 41 (2005)
13. X. Zhang, G. Zhang, L. Ying, W. Xiong, H. Han, Y. Wang, L. Rong, X. Xie, Z. Wang, Phys. C: Supercond. Appl. **548**, 1 (2018)
14. N.-H. Kim, H.-S. Kim, Y. Yang, X. Peng, D. Yu, Y.-J.Doh, arXiv preprint arXiv:1801.07855 (2018)
15. C. Tsuei, J. Kirtley, M. Rupp, J. Sun, A. Gupta, M. Ketchen, C. Wang, Z. Ren, J. Wang, M. Bhushan, in APS March Meeting Abstracts, (11996)
16. J. Kirtley, C. Tsuei, H. Raffy, Z. Li, A. Gupta, J. Sun, S. Megtert, EPL (Europhysics Letters) **36**, 707 (1996)
17. C. Tsuei, J.R. Kirtley, G. Hammerl, J. Mannhart, H. Raffy, Z. Li, Phys. Rev. Lett. **93**, 187004 (2004)
18. C. Tsuei, J. Kirtley, Phys. Rev. Lett. **85**, 182 (2000)
19. F. Rogeri, R. Zadorosny, P.N. Lisboa-Filho, E. Sardella, W. Ortiz, Supercond. Sci. Technol. **26**, 075005 (2013)
20. Ernst Helmut Brandt, Phys. Rev. B **72**, 024529 (2005)
21. Ernst Helmut Brandt, Phys. C: Supercond. Appl. **327**, 460 (2007)
22. R. John, Clem and Ernst Helmut Brandt. Phys. Rev. B **72**, 174511 (2005)
23. J. Barba-Ortega, J.L. Aguilar, J.D. González, Mod. Phys. Lett. B **28**(29), 1450230 (2014)
24. H. J. M. ter Brake, F.-Im. Buchholz G. Burnell, T. Claeson, D. Crété, P. Febvre, G. J. Gerritsma, H. Hilgenkamp, R. Humphreys, Z. Ivanov, W. Jutzi, M. I. Khabipov, J. Mannhart, H.-G. Meyer, J. Niemeyer, A. Ravex, H. Rogalla, M. Russo, J. Satchell, M. Siegel, H. Töpfer, F. H. Uhlmann, J.-C. Villögier, E. Wikborg, D. Winkler, A. B. Zorina, Phys. C: Supercond. Appl., **439**, 1 (2006)
25. T. Noh, A. Kindseth, V. Chandrasekhar, Appl. Phys. Express **14**, 103001 (2021)
26. Michiyasu Mori, Sadamichi Maekawa, Phys. Rev. B **104**, 064503 (2021)
27. C. Aguirre, A. de Arruda, J. Faundez, J. Barba-Ortega, Phys. B: Condens. Matter **615**, 413032 (2021)
28. J. Carlström, E. Babaev, M. Speight, Phys. Rev. B **83**, 174509 (2011)
29. M. Silaev, E. Babaev, Phys. Rev. B **85**, 134514 (2012)
30. E. Babaev, J. Carlström, M. Speight, Phys. Rev. Lett. **105**, 067003 (2010)
31. J. Barba-Ortega, E. Sardella, J.A. Aguiar, Phys. Lett. A. **379**, 732 (2015)
32. L. Komendova, M.V. Milosevic, A.A. Shanenko, F.M. Peeters, Phys. Rev. B **84**, 064522 (2011)
33. Yuriy Yerin, Stefan-Ludwig Drechsler, Phase solitons in a weakly coupled three-component superconductor, arxiv.org/abs/2103.17000
34. V.R. Misko, V.M. Fomin, J.T. Devreese, V.V. Moshchalkov, Phys. Rev. Lett. **90**, 147003 (2003)
35. P.C. Canfield, G.W. Crabtree, Phys. Today **56**, 34 (2003)
36. C. Aguirre, E. Sardella, J. Barba-Ortega, Solid. State. Comm. **306**, 113799 (2020)
37. T. Nunes, C. Aguirre, A. de Arruda, J. Barba, Eur. Phys. J. B **93**, 69 (2020)
38. E. Babaev, M. Speight, Phys. Rev. B. **72**, 180502 (2005)